

1 Magmatic activity in incipient continental break-up as revealed
2 by coupling melt and fluid inclusions

3 **G. Boudoire^{1,2}, N. Bobrowski^{3,4}, P.-Y. Burgi⁵, S. Calabrese^{2,6}, L. France^{7,8}, G. Giuffrida³, F.**
4 **Grassa², K. Karume⁹, J.-C. Kazadi Mwepu⁹, J. Kuhn¹⁰, R. Moritz¹¹, O. Munguiko**
5 **Munyamahoro^{1,9}, A. L. Rizzo^{12,13}, and D. Tedesco^{14,15,16}**

6 ¹*Université Clermont Auvergne, CNRS, IRD, OPGC, Laboratoire Magmas et Volcans, 6 avenue*
7 *Blaise Pascal, 63178 Aubière, France*

8 ²*Istituto Nazionale di Geofisica e Vulcanologia, Sezione di Palermo, Italy*

9 ³*Istituto Nazionale di Geofisica e Vulcanologia, Sezione di Catania, Italy*

10 ⁴*Institut für Umweltphysik, Ruprecht Karls University, Heidelberg, Germany*

11 ⁵*IT Department, University of Geneva, 1211 Genève, Switzerland.*

12 ⁶*DiSTeM, Università degli Studi di Palermo, Italy*

13 ⁷*Université de Lorraine, CNRS, CRPG, Nancy F-54000, France*

14 ⁸*Institut Universitaire de France, France*

15 ⁹*Observatoire Volcanologique de Goma, Democratic Republic of Congo*

16 ¹⁰*Department of Atmospheric and Oceanic Sciences, University of California, Los Angeles,*

17 *CA, USA*

18

19

20 © The Author(s) 2024. Published by Oxford University Press. All rights reserved. For

21 permissions, please e-mail: journals.permissions@oup.com.

22 ¹¹Department of Earth Science, University of Geneva, Rue des Maraîchers 13, CH 1205, Genève,

23 Switzerland

24 ¹²Dipartimento di Scienze dell'Ambiente e della Terra, Università degli Studi di Milano-Bicocca,

25 Piazza della Scienza 4, 20126 Milano, Italy

26 ¹³Istituto Nazionale di Geofisica e Vulcanologia, Sezione di Milano, Italy

27

28 ¹⁴DISTABIF, Università degli Studi della Campania "Luigi Vanvitelli", Caserta, Italy

29 ¹⁵Osservatorio Vesuviano, Istituto Nazionale di Geofisica e Vulcanologia, Naples, Italy

30 ¹⁶United Nations-MONUSCO, Goma, Republic Democratic of Congo.

31

32 **ABSTRACT**

33 Deciphering deep magmatic processes driving the onset of continental break-up is fundamental
34 to constrain our understanding of plate tectonics. The East African Rift System (EARS) is the
35 only currently active system on Earth to study distinct stages of rift evolution. We present a
36 coupled analysis of melt and fluid inclusions in the Virunga Volcanic Province (VVP) offering
37 an unprecedented insight into the dynamics of incipient rifting and its evolution. Our study
38 highlights that melting of distinct metasomes in the deep lithosphere is a common feature of
39 immature rifts. In the VVP, it leads to the emission of nephelinitic and basanitic melts at
40 Nyiragongo and Nyamulagira volcanoes, respectively. Additionally, the chemical composition of
41 melt and fluid inclusions supports the identification of another magmatic series in the area.
42 Related alkali basaltic melts would be produced by contemporary melting of a less enriched
43 domain in the upper lithosphere, more classically documented in mature rifts. Various extents of
44 mixing and crystallisation of these three distinct magmatic series occur in the lower crust beneath

45 the VVP where the barometric estimates are consistent with the presence of a thick seismic low
46 velocity zone (LVZ). The involvement of alkali basaltic melts in the regional magma production
47 could be also detected in the spread of gas emissions in the rift valley and in the fumaroles of the
48 main active volcanoes. Melting of the corresponding mantle domain is an added source of gas
49 release that may largely contribute to CO₂ emissions along the EARS.

50

51 INTRODUCTION

52 Magmatic activity in continental rifting handles some of the most remarkable volcanic
53 manifestations on Earth, including emission of hyperalkaline undersaturated and carbonatitic
54 volcanism (Rooney et al., 2020a), and massive CO₂ degassing (Wong et al., 2019). However, the
55 origin and evolution of the involved magmas as well as the architecture of associated magmatic
56 systems (especially the depth of magma ponding zones) are still poorly understood with respect
57 to other geodynamical contexts (Biggs et al., 2021).

58 The East African Rift System (EARS) is regarded as the current largest example of
59 continental break-up on Earth with magmato-tectonic events starting about 45 Myr on the
60 Eastern branch (Michon et al., 2022 and references therein). It evolved from trap-scale to plate-
61 scale rifting under the combined effect of an overall complex mantle upwelling dynamics and of
62 extensive stress acting on the African lithosphere (Michon et al., 2022). The origin of the large
63 chemical variability of associated lavas erupted is still a matter of debate, and several models
64 have been being formulated over the years, including various extents of mixing of distinct
65 components (Rooney et al., 2020a) such as (1) a convecting mantle with different mantle plumes
66 or thermal anomalies rooted in the African Large Low Shear Velocity Province, together with a
67 depleted mantle endmember (DMM) and (2) a sub-continental lithospheric mantle (SCLM) with

68 both a common lithospheric mantle (CLM) component partially metasomatized by the agents
69 extracted from the convecting mantle, and a Pan-African (PA) lithospheric domain that is
70 enriched in metasomes likely deriving from previous subduction events.

71 Magmatic activity on the Western branch started about 25 Myr ago and concentrated in
72 four main volcanic provinces, which are from North to South ([Michon et al. \(2022\)](#) and
73 [references therein](#)): Toro Ankole, Virunga, Kivu, and Rungwe. Carbonatitic, silica
74 undersaturated hyperalkaline and tholeiitic lavas are predominant with a prominent increase in
75 SiO₂ and depletion in K₂O from Toro Ankole to Kivu, which reflects a progressive decrease of
76 the melting depth towards the South ([Furman and Graham, 1999](#); [Rosenthal et al., 2009](#)). The
77 Virunga Volcanic Province (VVP) is currently the sole volcanic province of the Western branch
78 characterized by ongoing eruptive activity. The VVP is characterized by a massive gas release
79 from both volcanic gas plumes (CO₂, SO₂, and halogens) and soil degassing (CO₂) across the rift
80 valley ([Tedesco et al., 2010](#); [Bobrowski et al., 2017](#); [Fischer et al., 2019](#)). The VVP is also
81 known for its high potassic magmatism, making it one of the largest within-plate potassic
82 provinces on Earth ([Minissale et al., 2022](#)). Two main magmatic series are coexisting ([Pouclet et](#)
83 [al., 2016](#)): leucite bearing basanite and leucite-melilite bearing nephelinite. They are best
84 represented by the eruptive activity that occurred over 12 ka at the Nyamulagira and Nyiragongo
85 volcanoes, respectively. Previously, it has been proposed that those magmas were related to
86 mantle plume sources ([Chakrabarti et al., 2009](#); [Castillo et al., 2014](#)). Recent studies have rather
87 supported the melting of a heterogeneous metasomatized SCLM by thinning-driven adiabatic
88 decompression ([Pouclet et al., 2016](#); [Muravyeva et al., 2021](#); [Pitcavage et al., 2021](#); [Boudoire et](#)
89 [al., 2022](#); [Minissale et al., 2022](#)). However, the reason for the slight enrichment in primordial
90 helium (³He), leading to ³He/⁴He values higher than those expected from SCLM melting, in

91 some gaseous emissions along the Western branch is still poorly understood (Tassi et al., 2009;
92 Tedesco et al., 2010; Castillo et al., 2014; Boudoire et al., 2022).

93 Most studies that tried to elucidate the origin of the chemical variability of magmas in
94 continental rifting were based either on a compilation of bulk rock analyses for the entire EARS
95 or on the study of melt inclusions entrapped in crystals hosted by lavas from a single volcanic
96 edifice (see **Appendix A** for references). In this study, we present the analyses of both melt and
97 fluid inclusions from distinct eruptive centres in the VVP and discuss them in a global scheme
98 including earlier analyses of mafic melt inclusions obtained for other volcanic edifices along the
99 EARS (**Figure 1a**). This innovative approach of coupling information from melt (major, volatile,
100 and trace elements) and fluid (noble gases, barometry) inclusions from the same products offer a
101 unique opportunity to constrain magmatic processes in the VVP and more broadly those
102 involved in continental rifting.

103

104 **SAMPLING STRATEGY AND RESULTS**

105 **Lava flow samples**

106 Lavas flows from five eruptive sites were collected in the VVP (**Figure 1b**): a melilite
107 nephelinite from the Nyiragongo summit lava lake in 2020, a potassic basanite from the
108 Nyamulagira summit eruption in 2020, as well as two olivine nephelinite or melilitites samples
109 (Mudjoga, Kashaka), and an alkali basalt (Rumoka) from peripheral eruptive cones (<12 ka) in
110 the rift valley (Pouclet et al., 2016; Pouclet and Bram, 2021; Minissale et al., 2022; Molendijk et
111 al., 2024). The major element composition of the bulk rocks mostly overlaps within the chemical
112 variability previously documented in the area (**Figure 1c**), in particular the two main nephelinitic
113 and basanitic magmatic series reported in the VVP (Pouclet et al., 2016).

114

115 **Composition of melt and fluid inclusions**

116 Melt and fluid inclusions in olivine, clinopyroxene, and nepheline crystals from the collected
117 lava flows were analysed (see **Appendix A** for the full methodology and **Appendix B** for the
118 dataset). Melt and fluid inclusions in high (Fo_{87-90} ; where Fo is the forsterite content in molar
119 proportions), and low (Fo_{75-85}) magnesian olivine crystals were distinguished.

120 Three endmembers that frame the whole chemical variability in major, trace, and volatile
121 elements were identified (**Figure 2; Appendixes B and C**). (1) The “Nyiragongo-type”
122 nephelinitic melt exhibits the lowest Na_2O/K_2O (= 0.46), and the highest Cl (2352 ppm) and F
123 (4866 ppm) contents. The enrichment in more incompatible elements with respect to less
124 incompatible ones is significant ($La/Yb = 59.1$). Noble gases measurements are not reported due
125 to the existence of a diffusive loss and isotopic fractionation involving especially 3He and 4He .
126 (2) The “Nyamulagira-type” basanitic melt is characterized by $Na_2O/K_2O = 1.1$, high Cl (1249
127 ppm) and F (2145 ppm) contents as well as intermediate ratios between more incompatible and
128 less incompatible trace elements ($La/Yb = 37.1$). Noble gases systematics show relatively low
129 $^3He/^4He$ ($Rc/Ra = 7.8$), $^4He/^{40}Ar^*$ (= 0.2), but a high $CO_2/^3He$ (= 7.9×10^9). (3) The “Rumoka-
130 type” basaltic melt (in primitive Fo_{89-90} olivine crystals) is characterized by the highest
131 Na_2O/K_2O (= 1.4) and the lowest Cl (641 ppm) and F (1038 ppm) contents. The ratio between
132 light (LREE) and heavy (HREE) rare earth elements is the lowest ($La/Yb = 22.1$). Noble gases
133 show the highest $^3He/^4He$ ($Rc/Ra = 8.1$), $^4He/^{40}Ar^*$ (= 3.4), and lowest $CO_2/^3He$ (= 3.5×10^8).
134 Strong variations of highly incompatible elements ratios (such as Ce/Pb, Nb/La, Th/U, Zr/Hf) are
135 observed among these melts. The chemical composition of melt inclusions in olivine crystals
136 from the Mudjoga and Kashaka lavas ranges between a “Nyiragongo-type” nephelinitic melt and

137 a “Rumoka-type” basaltic melt (**Figure 2c, d; Appendix C**). The chemical composition of melt
138 and fluid inclusions in low magnesian olivine crystals from Rumoka lavas diverges from the
139 composition of a “Rumoka-type” basaltic melt towards a “Nyamulagira-type” basanitic melt
140 ([Head et al., 2011](#)).

141

142 **Barometric estimates**

143 The dissolved CO₂ content in melt inclusions ranges from 0.11-0.31 wt% in “Nyamulagira-type”
144 basanitic melt to 0.28-0.35 wt% in “Nyiragongo-type” nephelinitic melt and up to 1.69 wt% in
145 “Rumoka-type” basaltic melt. In melt inclusions from other peripheral products (Kashaka and
146 Mudjoga), the dissolved CO₂ content shows intermediate values (0.13-0.77 wt%) like the ones
147 (0.29-0.88 wt%) measured in the more evolved melt inclusions at Rumoka (Fo₈₃ olivine crystal).
148 The CO₂ density in fluid inclusions for these peripheral products ranges from 0.57 to 0.94 g/cc
149 (**Appendix B**).

150 Corresponding barometric estimates allow us to define four pressure ranges (**Figure 3**).

151 (1) The highest pressures (870-700 MPa) are recorded for Rumoka and Kashaka peripheral
152 products. Intermediate pressures are centred on two modes at (2) 540-450 MPa and (3) 230-330
153 MPa for Nyamulagira products (mirroring a differentiation trend from Fo_{79.6} to Fo_{75.6}) and for all
154 peripheral products. (4) The lowest pressures (70-130 MPa) are recorded in melt inclusions from
155 Nyiragongo (in nepheline crystals) and partially from Mudjoga. These barometric estimates
156 agree with earlier results based on petrological, geochemical, and geophysical methods
157 ([Louaradi et al., 1993](#); [Pouclet and Bram, 2021](#); [Molendijk et al., 2024](#)) which suggest at least
158 three major magma ponding zones beneath the VVP in similar pressure ranges.

159

160 **DISCUSSION**

161 For a single eruptive centre, the decrease in MgO, CaO/Al₂O₃, and Sc correlated to an increase in
162 incompatible elements such as K and Th suggest that olivine-clinopyroxene crystallisation
163 accounts for most of the chemical evolution in major and trace elements from the primitive to the
164 more evolved melt inclusions (**Figure 2a; Appendix C**). This predominant role of olivine-
165 clinopyroxene crystallisation (followed by feldspathoids in shallower magma reservoirs) in the
166 chemical variability was previously documented for lavas erupted in the surroundings of
167 Nyiragongo (Pitcavage et al., 2021; Molendijk et al., 2024). However, the crystallisation of the
168 main mineralogical phases reported in VVP magmas cannot explain the chemical variability
169 observed between the chemical endmembers (Minissale et al., 2019), nor that observed on
170 certain highly incompatible trace elements ratios (such as Th/U) between primitive and more
171 evolved melt inclusions at Rumoka. Our data also confirm that a significant role of crustal
172 contamination may be discarded consistently with the absence of Ce/Pb and Nb/La anomalies
173 (**Figure 2b; Chakrabarti et al., 2009; Minissale et al., 2022**) and thus in favour of heterogenous
174 mantle sources.

175

176 **Melting of metasomes in the deep lithospheric mantle**

177 The “Nyiragongo-type” nephelinitic melt has a clear affinity with a carbonatitic component (high
178 Zr/Hf and low Th/U, Ti/Eu), as previously suggested in the area (Chakrabarti et al., 2009;
179 Pouclet et al., 2016), and for nephelinitic melts emitted at Ol Doinyo Lengai (**Figure 2c;**
180 **Appendix C**). Lithium-enrichment in the “Nyamulagira-type” basanitic melt is consistent with a
181 preferential affinity for the global average of subducted sediment (GLOSS-II component) as
182 previously suggested also for the Bufumbira volcanic field in the VVP (**Figure 2d; Hudgins et**

183 al., 2015). While subducted sediments are thought to play a negligible role in the genesis of VVP
184 magmas (Minissale et al., 2022), past episodes of mantle metasomatism by slab-derived fluids
185 have led to preferential enrichment in some elements (Taniuchi et al., 2024), as attested by the
186 elevated Li/Yb in the Bufumbira volcanic field (Hudgins et al., 2015), and the lower $\delta^{13}\text{C}$ values
187 of CO_2 in gaseous emissions at Nyamulagira (Boudoire et al., 2022). The chemical composition
188 of melt inclusions also highlights a preferential signature of garnet over spinel (enrichment in
189 LREE and MREE with respect to HREE; **Figure 2e**) and of phlogopite over amphibole (low
190 Ba/Rb, $\text{Na}_2\text{O}/\text{K}_2\text{O}$ and high Rb/Sr; **Figure 2f**) in the mantle sources of the two related magmatic
191 series (Chakrabarti et al., 2009; Condomine et al., 2015; Muravyeva et al., 2021; Minissale et al.,
192 2022).

193 In summary, our new data from melt inclusions entirely agree with the melting of two
194 distinct types of metasomatized lithologies in the mantle beneath the Nyiragongo and
195 Nyamulagira volcanoes (“Type V magmas”; Rooney et al., 2020a). The generation of a
196 Nyiragongo primary olivine melilitic melt (leading to present nephelinitic melt by
197 differentiation) agrees with the melting of a carbonated metasome in the garnet-phlogopite-
198 carbonate stability field at depth >100 km, close to the base of the lithosphere (140-160 km-
199 depth; Chakrabarti et al., 2009; Muravyeva et al., 2021; Minissale et al., 2022). Conversely, a
200 distinct metasome affected by old slab fluids is expected to be at the origin of the Nyamulagira
201 primary basanitic melt (Chakrabarti et al., 2009; Minissale et al., 2022).

202

203 **Contemporary melting of an upper lithospheric mantle domain**

204 The chemical composition of melt inclusions analysed in this study also clearly highlights the
205 contemporary production of a third magmatic series (the “Rumoka-type” basaltic melt) not yet

206 documented in the VVP but reminiscent of “Type IIb magmas” (Rooney et al., 2020a). The
207 similarity of chemical compositions in trace elements between the related melt inclusions and
208 those from the 2011 eruption at Nabro in the Afar region is striking (Figure 2; Appendix C).
209 These melts are ubiquitous along the EARS and are considered to be produced at the beginning
210 of the transition towards mature rifts by thermobaric destabilization of a thick lithosphere
211 (Rooney et al., 2020a, 2020b; Chiasera et al., 2021). Along the Western branch, these melts
212 would be produced by melting of a less enriched lithospheric mantle domain (Chakrabarti et al.,
213 2009; Rosenthal et al., 2009; Pouclet et al., 2016).

214 The $\text{Na}_2\text{O}/\text{K}_2\text{O}$ ratio above the unit in the primitive basaltic melt inclusions at Rumoka
215 suggests the presence of amphibole (together with phlogopite) in the mantle source, a mineral
216 characteristic of a shallower lithospheric melting domain (60-80 km-depth; Rosenthal et al.,
217 2009; Muravyeva et al., 2021). The melting of a similar shallow mantle domain was consistently
218 proposed for the genesis of alkali basalts of similar composition in the neighbouring Kivu
219 volcanic province (Rosenthal et al., 2009) and in the genesis of Type IIb magmas (Rooney et al.,
220 2020a). In the VVP, it supports the idea of contemporary melting of distinct lithospheric mantle
221 domains involved in magma genesis. A heterogeneous SCLM with a deeper lithospheric mantle
222 hosting metasomes (U-Th enriched lithologies) and a less enriched upper lithospheric mantle
223 could be a reasonable explanation for the slight $^3\text{He}/^4\text{He}$ variability seen between Nyiragongo,
224 Nyamulagira, and Rumoka products. This hypothesis agrees with the observation that
225 metasomatized lithologies are preferentially found near the base of the lithosphere along the
226 EARS (Rooney et al., 2020a). Such vertical partition has also been suggested beneath the North
227 Tanzanian Divergence (NTZ) of the Eastern branch, where a LVZ has been imaged at a mid-
228 lithospheric depth (~60 km) separating the two mantle components (Plasman et al., 2017).

229 Whatever the case, the $^3\text{He}/^4\text{He}$ values remain within the range of values classically attributed to
230 the DMM (8 ± 1 Ra; [Tedesco et al., 2010](#)) and confirm the major contribution of the upper mantle
231 in the genesis of the fluids under this part of the EARS ([Aiuppa et al., 2021](#); [Boudoire et al.,](#)
232 [2022](#)).

233

234 **Magma mixing of distinct magmatic series**

235 The primitive melt inclusions entrapped in the deepest roots of the magmatic systems beneath the
236 VVP, i.e. at the crust-mantle transition zone ([Muravyeva et al., 2021](#)) (**Figure 3**), and those of
237 Nyiragongo and Nyamulagira, better preserve the chemical signature of distinct magmatic series.
238 Conversely, more evolved melt inclusions from peripheral eruptive vents have a hybrid chemical
239 composition between these magmatic series (**Figure 2**). We suggest that this fingerprint results
240 from variable mixing of the distinct identified magmatic series in intermediate crustal magma
241 ponding zones. In fact, we document two intermediate crustal pressure modes (540-450 MPa and
242 230-330 MPa) for these peripheral products (**Figure 3**) that match with the top of the LVZs
243 beneath the VVP ([Mavonga et al., 2010](#); [Poucllet and Bram, 2021](#)) with the main one extending
244 from 18 to 28 km depth ([Muravyeva et al., 2021](#)). These LVZs image magma reservoirs or
245 several melt-rich sills where magma mixing is eased ([Muravyeva et al., 2021](#)). Complex crystal
246 zoning and textures reported in some peripheral lavas ([Molendijk et al., 2024](#)) partially highlight
247 this mixing process. A similar LVZ linked to magmatic processes has also been imaged in the
248 lower crust (15-35 km depth) beneath the NTZ of the Eastern branch ([Plasman et al., 2017](#)).

249

250 **Insights on current degassing processes**

251 Nyiragongo and Nyamulagira are among the strongest volcanic gas emitters on Earth (Fischer et
252 al., 2019). Degassing paths modelled from the initial composition of melt inclusions (see
253 **Appendix A** for the methodology) were compared to the temporal evolution of CO₂/SO₂ and
254 Cl/S from gas plumes composition reported in literature (Bobrowski et al., 2017; Boudoire et al.,
255 2022). This period overlaps with the progressive replenishment of the Nyiragongo lava lake
256 between the two flank eruptions in 2002 and 2021 (Burgi et al., 2020) and the renewal of lava
257 lake activity at Nyamulagira since 2012 (Burgi et al., 2021). The increase in CO₂/SO₂ and Cl/S
258 values suggests that magma arrival and degassing in the deeper crustal magmatic reservoirs
259 (>250 MPa) prevail on magma degassing in the shallowest ones (<150 MPa; **Figure 4a, b**) over
260 time. At Nyiragongo, the existence of various degassing magmatic sources involved in the
261 outgassing of the lava lake was previously proposed (Bobrowski et al., 2017) and the exceptional
262 occurrence of deep mush material in the 2021 lava from Nyiragongo (Molendijk et al., 2024)
263 supports this hypothesis.

264 We also note that the ³He/⁴He values in Nyiragongo fumaroles may have been slightly
265 lower in 2020 (Rc/Ra = 7.3±0.2) (Boudoire et al., 2022), preceding the 2021 flank eruption than
266 during the 2003-2007 period (Rc/Ra = 7.8±0.8 and up to 8.7; Tedesco et al., 2010) (**Figure 4c**).
267 This behaviour mirrors the increase of magma flux feeding the lava lake on the same time span
268 (Burgi et al., 2020, 2021). This slight decrease in ³He/⁴He values over time, which does not
269 depend on pressure (and is therefore not linked to the deepening of the degassing magmatic
270 sources over time), highlights a potential ⁴He-enrichment from 2003 to 2020. It could reflect an
271 increase of the magma production (and influx) from the Nyiragongo deep metasomatized mantle
272 source that is enriched in U-Th (and thus ⁴He) with respect to the other endmembers described in
273 this study. Conversely, it is worth noting the chemical affinity (higher Rc/Ra and ⁴He/⁴⁰Ar*

274 coupled with low $\text{CO}_2/{}^3\text{He}$ and $\delta^{13}\text{C}$ of regional dry CO_2 gas emissions (e.g., mazuku on **Figure**
275 **4c**) from the rift valley with the isotopic signature of fluid inclusions in crystals from Rumoka
276 products. High ${}^4\text{He}/{}^{40}\text{Ar}^*$ and low $\text{CO}_2/{}^3\text{He}$ and $\delta^{13}\text{C}$ are reminiscent of more degassed magmas
277 ([Boudoire et al., 2022](#)) and may suggest that steady-state outgassing through the rift valley is
278 mostly linked to magma storage and degassing in the LVZs that could be preferentially fed by
279 the melting of the upper and less enriched lithospheric mantle domain ([Tedesco et al., 2010](#);
280 [Boudoire et al., 2022](#)).

281

282 CONCLUSIONS

283 Melt and fluid inclusions suggest that current magma production beneath the VVP is not solely
284 linked to the melting of various mantle metasomes that preferentially feed the main volcanic
285 edifices, as documented for immature rifts ([Rooney et al., 2020a](#); [Aiuppa et al., 2021](#)). The
286 contemporary melting of a less enriched lithospheric domain, isolated at a shallower level in the
287 mantle, is shown by the composition of primitive melt inclusions from peripheral products
288 erupted in the rift valley. This process is rather reminiscent of magmatic production at the
289 beginning of the transition towards mature rifts. We propose that steady-state degassing
290 associated with continental rifting in the area is preferentially triggered by magma production in
291 the upper part of the lithosphere (at 60-80 km-depth), followed by mixing and storage of the melt
292 in the lower crust (at 15-35 km-depth), where LVZs are imaged, rather than by the melting of
293 isolated deep lithospheric metasomes ([Muirhead et al., 2020](#); [Aiuppa et al., 2021](#)). This model
294 would preferentially account for global CO_2 emissions along the EARS with respect to volcanic
295 emissions ([Wong et al., 2019](#)) and for the large chemical variability of erupted melts ([Rooney et](#)
296 [al., 2020a](#)).

297 **SUPPLEMENTARY MATERIAL AND DATA AVAILABILITY STATEMENT**

298 The Supplemental Material is composed of four appendixes. **Appendix A** describes the
299 methodology used in this study. It provides details about the analytical conditions of
300 measurements, data treatment, degassing models, and comparative data from literature.
301 **Appendix B** is the complete dataset of measurements acquired for this study. **Appendix C** is
302 composed of four complementary figures that sustain the discussion about the role of
303 crystallisation, contamination, mixing processes, and mantle sources lithologies in the chemical
304 variability of melt inclusions. **Appendix D** is the completed repository template available on a
305 recognized domain repository of the GFZ Data Services through the link [https://dataservices.gfz-](https://dataservices.gfz-potsdam.de/panmetaworks/review/0987bbb94d29daa7e406e048ef73614579375334e467578be75da9e606a69d78/)
306 [potsdam.de/panmetaworks/review/0987bbb94d29daa7e406e048ef73614579375334e467578be75](https://dataservices.gfz-potsdam.de/panmetaworks/review/0987bbb94d29daa7e406e048ef73614579375334e467578be75da9e606a69d78/)
307 [da9e606a69d78/](https://dataservices.gfz-potsdam.de/panmetaworks/review/0987bbb94d29daa7e406e048ef73614579375334e467578be75da9e606a69d78/) with a reserved (and not yet registered at this step) DOI
308 (<https://doi.org/10.5880/fidgeo.2024.029>) (Boudoire, 2024) for accessing the dataset and the data
309 description in accordance with the data availability statement.

310
311 **ACKNOWLEDGMENTS**

312 We are grateful to the Goma Volcano Observatory (OVG) for the invitation and logistic help.
313 The United Nations program of MONUSCO is warmly thanked for the great support in the field
314 deployment by helicopter. The ICCN is acknowledged for providing the logistic inside the
315 National Park of Virunga. The SVG team is thanked for their priceless support in the
316 coordination of the descent into the craters. We are in debt with M. Benbakkar, J.-L. Devidal, C.
317 Fonquernie, F. Schiavi, E. Voyer at the LMV, M. Champenois at the CRPG, E. Rose-Koga at
318 ISTO, and M. Tantillo at the INGV for their assistance during sample preparation and analysis.
319 T. Rooney, A.Z. Tadesse, and V. Zanon are acknowledged for their constructive review of the

320 article. This research was funded by the Italian initiative Pianeta Dinamico 2023-2025 through
321 the MUSUNGU project and by the French Government Laboratory of Excellence initiative n°
322 ANR-10-LABX-0006, the Region Auvergne and the European Regional Development Fund
323 through the project DegazRift. D. Tedesco was funded by the UN-MONUSCO during this
324 project. This is contribution no. XXX of the ClerVolc program of the International Research
325 Center for Disaster Sciences and Sustainable Development of the University Clermont
326 Auvergne.

327

328 REFERENCES CITED

329 Aiuppa, A., Casetta, F., Coltorti, M., Stagno, V., & Tamburello, G. (2021). Carbon concentration
330 increases with depth of melting in Earth's upper mantle. *Nature Geoscience*, 14(9), 697-703.

331

332 Biggs, J., Ayele, A., Fischer, T. P., Fontijn, K., Hutchison, W., Kazimoto, E., ... & Wright, T. J.
333 (2021). Volcanic activity and hazard in the East African Rift Zone. *Nature*
334 *communications*, 12(1), 6881.

335

336 Bobrowski, N., Giuffrida, G. B., Yalire, M., Lübcke, P., Arellano, S., Balagizi, C., ... & Tedesco,
337 D. (2017). Multi-component gas emission measurements of the active lava lake of Nyiragongo,
338 DR Congo. *Journal of African Earth Sciences*, 134, 856-865.

339

340 Boudoire, G. (2024). Dataset of lava samples, melt and fluid inclusions analysis from the
341 Virunga Volcanic Province (DR Congo). GFZ Data Services.
342 <https://doi.org/10.5880/fidgeo.2024.029>.

343 Boudoire, G., Giuffrida, G., Liuzzo, M., Bobrowski, N., Calabrese, S., Kuhn, J., ... & Tedesco,
344 D. (2022). Chemical variability in volcanic gas plumes and fumaroles along the East African Rift
345 System: New insights from the Western Branch. *Chemical Geology*, 596, 120811.

346
347 Burgi, P. Y., Boudoire, G., Rufino, F., Karume, K., & Tedesco, D. (2020). Recent activity of
348 Nyiragongo (Democratic Republic of Congo): New insights from field observations and
349 numerical modeling. *Geophysical Research Letters*, 47(17), e2020GL088484.

350
351 Burgi, P. Y., Valade, S., Coppola, D., Boudoire, G., Mavonga, G., Rufino, F., & Tedesco, D.
352 (2021). Unconventional filling dynamics of a pit crater. *Earth and Planetary Science*
353 *Letters*, 576, 117230.

354
355 Castillo, P. R., Hilton, D. R., & Halldórsson, S. A. (2014). Trace element and Sr-Nd-Pb isotope
356 geochemistry of Rungwe Volcanic Province, Tanzania: implications for a superplume source for
357 East Africa Rift magmatism. *Frontiers in Earth Science*, 2, 21.

358
359 Chakrabarti, R., Basu, A. R., Santo, A. P., Tedesco, D., & Vaselli, O. (2009). Isotopic and
360 geochemical evidence for a heterogeneous mantle plume origin of the Virunga volcanics,
361 Western rift, East African Rift system. *Chemical Geology*, 259(3-4), 273-289.

362
363 Chiasera, B., Rooney, T. O., Bastow, I. D., Yirgu, G., Grosfils, E. B., Ayalew, D., ... & Ramsey,
364 M. (2021). Magmatic rifting in the Main Ethiopian Rift began in thick continental lithosphere;
365 the case of the Galema Range. *Lithos*, 406, 106494.

366 Condomines, M., Carpentier, M., & Ongendangenda, T. (2015). Extreme radium deficit in the
367 1957 AD Mugogo lava (Virunga volcanic field, Africa): Its bearing on olivine-melilitite
368 genesis. *Contributions to Mineralogy and Petrology*, 169, 1-19.

369
370 Fischer, T. P., Arellano, S., Carn, S., Aiuppa, A., Galle, B., Allard, P., ... & Chiodini, G. (2019).
371 The emissions of CO₂ and other volatiles from the world's subaerial volcanoes. *Scientific*
372 *reports*, 9(1), 18716.

373
374 Furman, T., & Graham, D. (1999). Erosion of lithospheric mantle beneath the East African Rift
375 system: geochemical evidence from the Kivu volcanic province. In *Developments in*
376 *Geotectonics* (Vol. 24, pp. 237-262). Elsevier.

377
378 Head, E. M., Shaw, A. M., Wallace, P. J., Sims, K. W., & Carn, S. A. (2011). Insight into
379 volatile behavior at Nyamuragira volcano (DR Congo, Africa) through olivine-hosted melt
380 inclusions. *Geochemistry, Geophysics, Geosystems*, 12(10).

381
382 Hudgins, T. R., Mukasa, S. B., Simon, A. C., Moore, G., & Barifaijo, E. (2015). Melt inclusion
383 evidence for CO₂-rich melts beneath the western branch of the East African Rift: implications
384 for long-term storage of volatiles in the deep lithospheric mantle. *Contributions to Mineralogy*
385 *and Petrology*, 169, 1-18.

386
387 Louaradi, D., Clochiatti, R., Pineau, F., & Javoy, M. (1993). Magma storage beneath Nyiragongo
388 volcano (Zaire): Evidence from fluid and melt inclusions. In *Terra Abstracts* (Vol. 5, p. 573).

389 Mavonga, T., Zana, N., & Durrheim, R. J. (2010). Studies of crustal structure, seismic precursors
390 to volcanic eruptions and earthquake hazard in the eastern provinces of the Democratic Republic
391 of Congo. *Journal of African Earth Sciences*, 58(4), 623-633.

392
393 Michon, L., Famin, V., & Quidelleur, X. (2022). Evolution of the East African Rift System from
394 trap-scale to plate-scale rifting. *Earth-Science Reviews*, 231, 104089.

395
396 Minissale, S., Casalini, M., Cucciniello, C., Balagizi, C., Tedesco, D., Boudoire, G., ... &
397 Melluso, L. (2022). The geochemistry of recent Nyamulagira and Nyiragongo potassic lavas,
398 Virunga Volcanic Province, and implications on the enrichment processes in the mantle
399 lithosphere of the Tanzania-Congo craton. *Lithos*, 420, 106696.

400
401 Minissale, S., Zanetti, A., Tedesco, D., Morra, V., & Melluso, L. (2019). The petrology and
402 geochemistry of Nyiragongo lavas of 2002, 2016, 1977 and 2017 AD, and the trace element
403 partitioning between melilitite glass and melilite, nepheline, leucite, clinopyroxene, apatite,
404 olivine and Fe-Ti oxides: a unique scenario. *Lithos*, 332, 296-311.

405
406 Molendijk, S. M., Namur, O., Kamate Kaleghetso, E., Mason, P. R., Smets, B., Vander Auwera,
407 J., & Neave, D. A. (2024). Plumbing system architecture and differentiation processes of the
408 Nyiragongo volcano, DR Congo. *Journal of Petrology*, 65(01), egad088.

409

410 Muirhead, J. D., Fischer, T. P., Oliva, S. J., Laizer, A., van Wijk, J., Currie, C. A., ... & Ebinger,
411 C. J. (2020). Displaced cratonic mantle concentrates deep carbon during continental
412 rifting. *Nature*, 582(7810), 67-72.

413
414 Muravyeva, N. S., Senin, V. G., Ivanov, A. V., & Belyatsky, B. V. (2021). Leucite basanites of
415 Virunga (east African rift): some insights into petrogenesis and source composition. *Lithos*, 384,
416 105972.

417
418 Pitcavage, E., Furman, T., Nelson, W. R., Kalegga, P. K., & Barifajjo, E. (2021). Petrogenesis of
419 primitive lavas from the Toro Ankole and Virunga Volcanic Provinces: Metasomatic mineralogy
420 beneath East Africa's Western Rift. *Lithos*, 396, 106192.

421
422 Plasman, M., Tiberi, C., Ebinger, C., Gautier, S., Albaric, J., Peyrat, S., ... & Gama, R. (2017).
423 Lithospheric low-velocity zones associated with a magmatic segment of the Tanzanian Rift, East
424 Africa. *Geophysical Journal International*, 210(1), 465-481.

425
426 Pouclet, A., Bellon, H., & Bram, K. (2016). The Cenozoic volcanism in the Kivu rift:
427 Assessment of the tectonic setting, geochemistry, and geochronology of the volcanic activity in
428 the South-Kivu and Virunga regions. *Journal of African Earth Sciences*, 121, 219-246.

429
430 Pouclet, A., & Bram, K. (2021). Nyiragongo and Nyamuragira: a review of volcanic activity in
431 the Kivu rift, western branch of the East African Rift System. *Bulletin of Volcanology*, 83(2), 10.

432

433 Rooney, T. O. (2020a). The Cenozoic magmatism of East Africa: part V—magma sources and
434 processes in the East African Rift. *Lithos*, 360, 105296.

435
436 Rooney, T. O. (2020b). The Cenozoic magmatism of East Africa: part IV—the terminal stages of
437 rifting preserved in the Northern East African Rift System. *Lithos*, 360, 105381.

438
439 Rosenthal, A., Foley, S. F., Pearson, D. G., Nowell, G. M., & Tappe, S. (2009). Petrogenesis of
440 strongly alkaline primitive volcanic rocks at the propagating tip of the western branch of the East
441 African Rift. *Earth and Planetary Science Letters*, 284(1-2), 236-248.

442
443 Taniuchi, H., Kawamoto, T., Nakatani, T., Ishizuka, O., Suzuki, T., & Tomiya, A. (2024).
444 Compositional evolution of slab-derived fluids during ascent: implications from trace-element
445 partition between hydrous melts and Cl-free or Cl-rich aqueous fluids. *Contributions to*
446 *Mineralogy and Petrology*, 179(5), 51.

447
448 Tassi, F., Vaselli, O., Tedesco, D., Montegrossi, G., Darrah, T., Cuoco, E., ... & Delgado
449 Huertas, A. (2009). Water and gas chemistry at Lake Kivu (DRC): Geochemical evidence of
450 vertical and horizontal heterogeneities in a multibasin structure. *Geochemistry, Geophysics,*
451 *Geosystems*, 10(2).

452
453 Tedesco, D., Tassi, F., Vaselli, O., Poreda, R. J., Darrah, T., Cuoco, E., & Yalire, M. M. (2010).
454 Gas isotopic signatures (He, C, and Ar) in the Lake Kivu region (western branch of the East

455 African rift system): Geodynamic and volcanological implications. *Journal of Geophysical*
456 *Research: Solid Earth*, 115(B1).

457

458 Wong, K., Mason, E., Brune, S., East, M., Edmonds, M., & Zahirovic, S. (2019). Deep carbon
459 cycling over the past 200 million years: a review of fluxes in different tectonic settings. *Frontiers*
460 *in Earth Science*, 7, 263.

461

462

463

464

465

466

467

468

469

470

471

472

473

474

475

476

477

478 **FIGURE CAPTIONS**

479

480 **Figure 1.** (A) Location of the volcanoes of the East African Rift System (EARS) for which basic
481 melt inclusions were documented and compiled in this study. Continuous lines show the main
482 EARS active segments (Michon et al., 2022). (B) Location of the sampling sites in the Virunga
483 Volcanic Province (VVP) for the melt and fluid inclusions investigation of this study. (C)
484 Composition of the host lavas (coloured dots refer to the lava sampled in the VVP) and
485 comparison with literature data (coloured fields refer to the lava sampled along the EARS, see
486 **Appendix A** for references).

487

488 **Figure 2.** (A) SiO_2 vs. K_2O in melt inclusions with the composition of the main mineralogic
489 phases in the VVP indicated with crosses (Cpx. stands for clinopyroxene). (B) Nb/La vs. Ce/Pb,
490 (C) Zr/Hf vs. Th/U, and (D) Li/Yb vs. Nb/U in melt inclusions compared with the composition
491 of global endmembers showed with squares (see **Appendix A** for references). (E) K/Yb vs.
492 Dy/Yb and (F) Ba/Rb vs. Rb/Sr in melt inclusions with the expected effect of amphibole,
493 phlogopite, garnet and spinel in the melted mantle source (Furman and Graham, 1999; Duggen et
494 al., 2005). Numbers show the melting degree on the theoretical mantle sources melting paths.
495 Coloured fields refer to the composition of basic melt inclusions from the EARS documented in
496 the literature (see **Appendix A** for references).

497

498 **Figure 3.** Pressure and depth estimates of magma ponding zones beneath the VVP from CO_2
499 densimetry in fluid inclusions (FI) and CO_2 - H_2O equilibrium in melt inclusions (MI). Earlier
500 data from literature (Lit.) for Nyamulagira and Nyiragongo about potential magma ponding

501 zones (shaded coloured ellipsoids) and the crust structure (low velocity zones, crust-mantle
502 transition zone) are listed in **Appendix A**. The melt inclusions selected as chemical endmembers
503 in this study are highlighted: (1) for Nyiragongo-type melt, (2) for Nyamulagira-type melt, and
504 (3) for Rumoka-type melt.

505

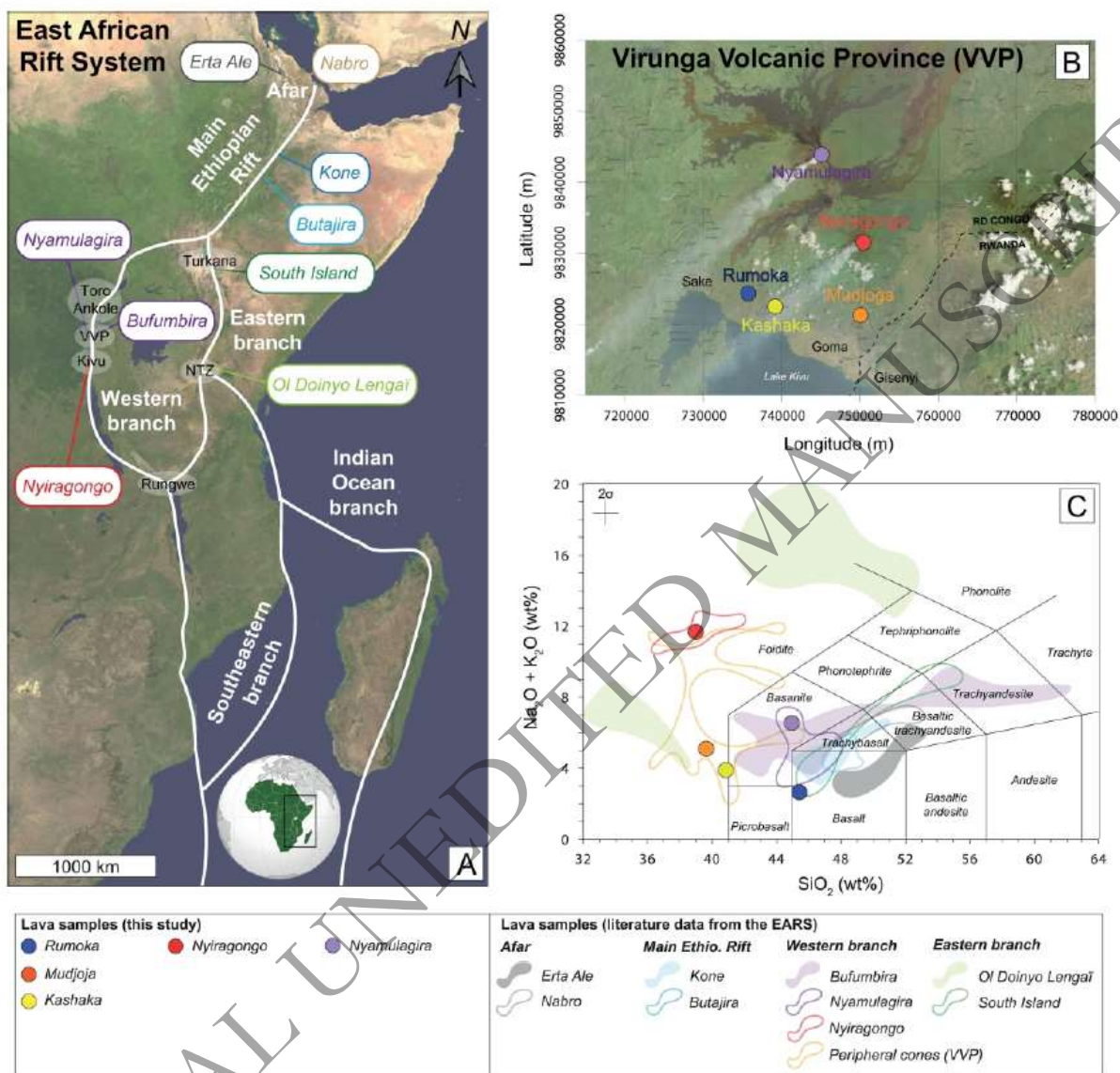
506 **Figure 4.** Pressure-dependence of CO₂/SO₂ and Cl/S molar ratios in gas plumes emitted at (A)
507 Nyiragongo and (B) Nyamulagira. Degassing paths were modelled using SulfurX (Ding et al.,
508 2023) and SolEx (Witham et al., 2012) considering both Fractional Equilibrium Degassing
509 (FED) and Batch Equilibrium Degassing (BED). See **Appendix A** for more details about starting
510 conditions and parameters used in the modelling. Values framed on the x-axis highlight (i)
511 averaged measurements made in volcanic gas plumes from 2005 to 2014 (Sawyer et al. 2008;
512 Bobrowski et al., 2017a, b) and (ii) minimum and maximum values measured in 2020 (Boudoire
513 et al., 2022). The theoretical pressure ranges corresponding to these measurements are highlighted
514 on the y-axis (shaded boxes) as well as the corresponding magma ponding zones (circles) from
515 **Figure 2.** (C) CO₂/³He vs. Rc/Ra in fluid inclusions with dashed black lines evidencing mixing
516 of a mantle endmember (Rumoka-type melt) and various crustal components (Barry et al., 2013).
517 The stars show the average composition of the fumaroles at Nyiragongo and Nyamulagira
518 (Tedesco et al., 2010; Boudoire et al., 2022). CO₂/³He vs. Th/U with dashed lines showing
519 mixing between (1) a Nyiragongo-type melt and either (2) a Nyamulagira-type melt or (3) a
520 Rumoka-type melt.

521

522

523

524 Fig. 1.



525

526

527

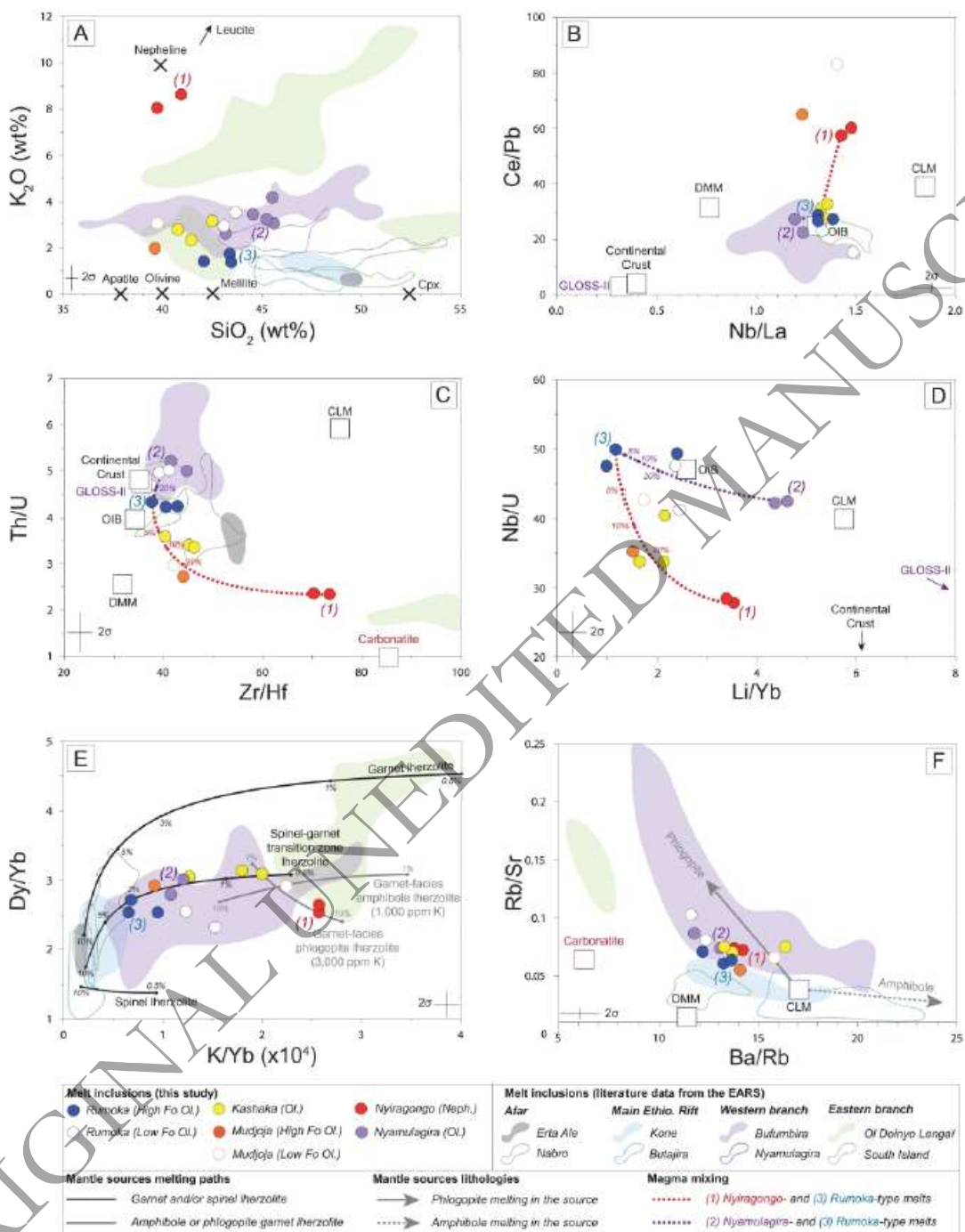
528

529

530

531

532 Fig. 2.



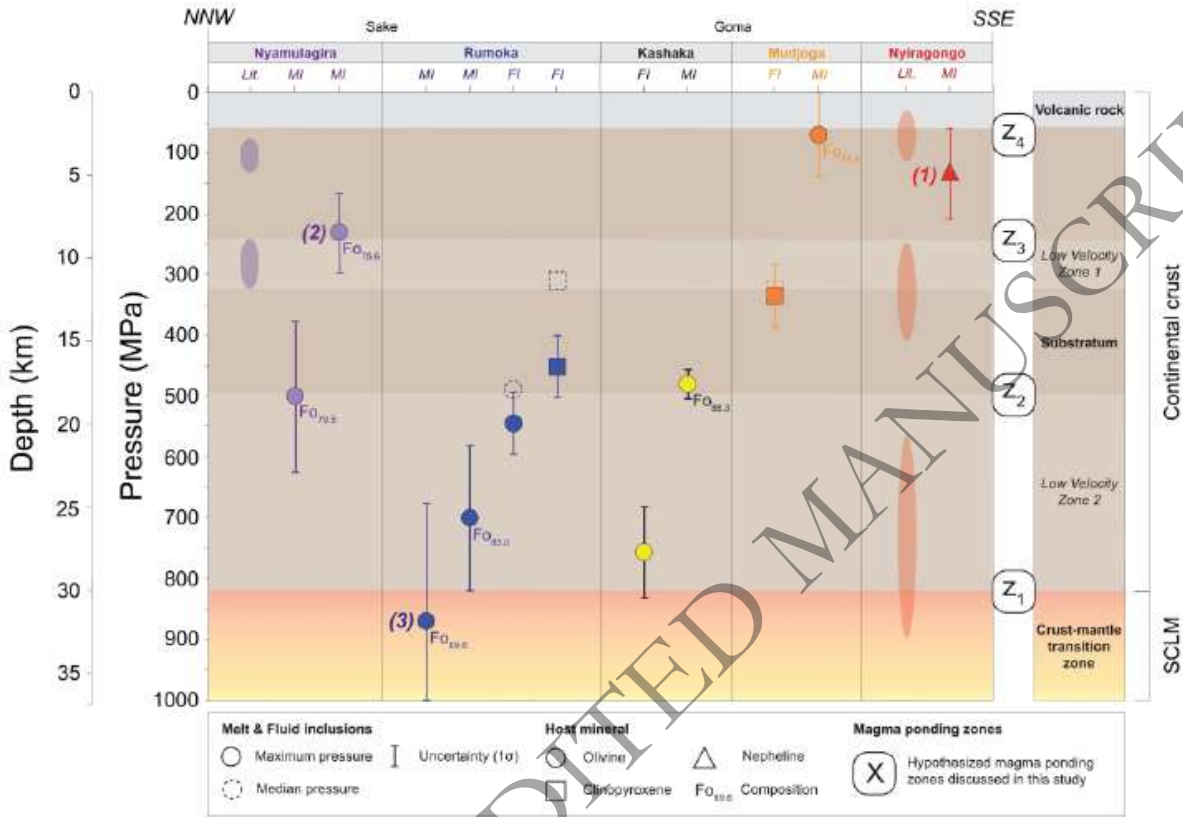
533

534

535

536

537 **Fig. 3.**



538

539

540

541

542

543

544

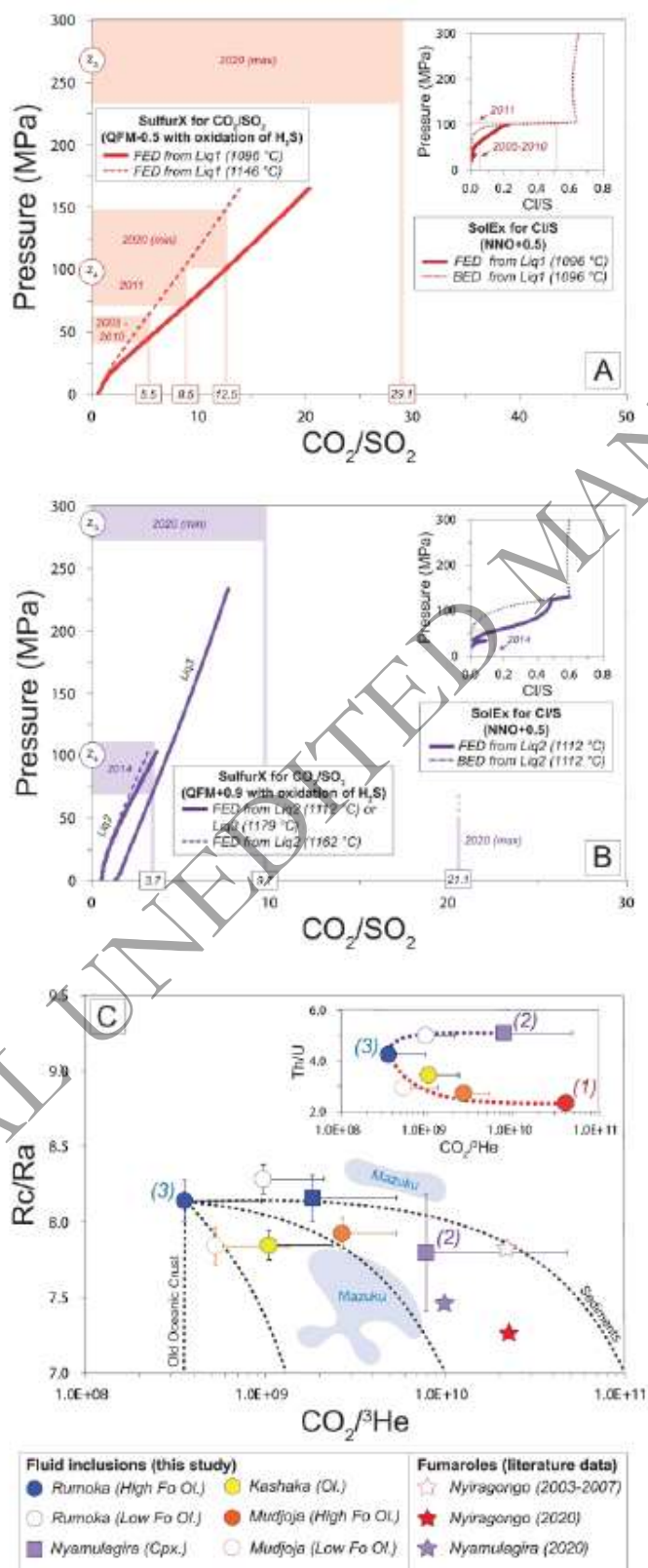
545

546

547

548

549 Fig. 4.





Deltech Furnaces

Sustained operating
temperatures to 1800°
Celsius

www.deltechfurnaces.com



Gas Mixing System



An ISO 9001:2015 certified company

Custom Vertical Tube



ASME NQA-1 2008 Nuclear Quality Assurance

Standard Vertical Tube



Control systems are certified by Intertek UL508A compliant

Bottom Loading Vertical Tube